Absorption Cross Sections and Self-Reaction Kinetics of the IO Radical

Matthew H. Harwood,[†] James B. Burkholder,*[,†] Martin Hunter,[‡] R. W. Fox,[§] and A. R. Ravishankara*[,⊥]

Aeronomy Laboratory, National Oceanic and Atmospheric Administration, 325 Broadway, Boulder, Colorado 80303

Received: August 9, 1996; In Final Form: October 30, 1996[⊗]

Rate coefficients for the IO self-reaction, IO + IO → products (4), were determined over the range 250−320 K and were found to be independent of temperature with an average value of $(9.9 \pm 1.5) \times 10^{-11}$ cm^3 molecule^{-1} s^{-1}. Absorption cross sections for the IO radical were measured between 340 and 480 nm. The absorption cross section at the peak of the (4,0) band was determined as a function of temperature. The cross section is essentially independent of temperature with an average value between 373 and 203 K of $(3.6 \pm 0.5) \times 10^{-17}$ cm^2 molecule^{-1}. Comparison with previous measurements and a discussion of the atmospheric implications of these results are also presented.

1. Introduction

The importance of iodine-containing compounds to the chemistry of the atmosphere has long been debated.[1−4] The most significant single source of iodine-containing species in the atmosphere is methyl iodide (produced naturally by marine biota and released in industrial pollution), and field measurements show[3] that its concentration in the boundary layer ranges between 1 and 50 pptv.

CH_3I is rapidly photolyzed in the troposphere to release iodine atoms which can react with ozone to yield IO:

$$I + O_3 \rightarrow IO + O_2 \quad (1)$$

The atmospheric fate of IO is primarily determined by the rates of its photolysis (2) and the reactions of IO (3) with a variety of other atmospheric species.

$$IO + h\nu \rightarrow I + O \quad (2)$$

$$IO + X \rightarrow \text{products } (X = NO, NO_2, HO_2, IO, ClO, BrO) \quad (3)$$

If reaction 3 produces I atoms (or produces a species that can lead to I) without producing an oxygen atom, then catalytic destruction of ozone can occur through reactions 1 and 3. However, IO can be converted to inactive "reservoir" compounds (e.g., HOI, HI, and $IONO_2$) in reaction 3. These compounds are longer lived and can be removed from the atmosphere by aerosol scavenging or rainout. Relative to the other halogens, the formation of iodine reservoir compounds is believed to be very inefficient, and thus the fraction of the total iodine expected to be in active forms is large, much greater than for chlorine and bromine.[5]

It is believed [3] that the most important reactions for iodine-catalyzed ozone loss in the troposphere are the following:

$$IO + IO \rightarrow \rightarrow 2I + O_2 \quad (4)$$

and

$$IO + HO_2 \rightarrow HOI + O_2 \quad (5)$$

$$HOI + h\nu \rightarrow I + HO \quad (6)$$

Davis et al.[4] have calculated the effect of these iodine reactions on ozone destruction rates in the troposphere for different CH_3I mixing ratios using the data available to them. With 7 pptv of CH_3I in their model, the inclusion of the iodine chemistry increased the rate of total tropospheric column ozone loss by 30%. The contribution of the iodine-catalyzed loss processes increased with altitude as the efficiency of other destruction cycles (mainly HO_x chemistry) decreased. As the concentrations of CH_3I in the model increased, so did the importance of the IO self-reaction relative to reactions 5 and 6. Measurements of CH_3I over the Pacific Ocean[4] have demonstrated that the vertical profiles of CH_3I show interesting features. The mixing ratio decreases from sea level to about 6 km but then shows an increase to values of between 0.1 and 1 pptv at about 12 km. This suggests a role for iodine in the upper as well as lower troposphere. In addition, enhanced concentrations of halogens in the marine boundary layer in springtime (observed in the Polar Sunrise Experiment[6]) coincide with episodic and rapid depletion of ozone in arctic regions. Iodine compounds, in addition to (or together with) bromine, could also play a role in these events.

It is clear that IO can have a significant impact on tropospheric ozone, but recent work by Solomon et al.[5] has suggested that atmospheric iodine-containing species may also significantly impact the ozone chemistry of the lower stratosphere at mid-latitudes. In this region dramatic downward trends in ozone concentrations have been observed during the past two decades.[7] Although the tropospheric lifetime of CH_3I (with respect to photolysis) is short, it is believed that strong convective processes can provide fast transport of CH_3I into the upper troposphere and subsequently into the stratosphere.

The potential impact of iodine-containing species on stratospheric ozone is crucially dependent upon the concentration of the iodine compounds in this region and upon the rate coefficients and reaction products for a few important chemical reactions. It is unlikely that the concentrations of iodine species

[†] Cooperative Institute for Research in Environmental Sciences, University of Colorado, Boulder, CO 80309.
[‡] Phillips Laboratory, Hanscom Air Force Base, Massachusetts.
[§] National Institute for Standards and Technology, 325 Broadway, Boulder, Colorado, 80303.
[⊥] Also associated with the Department of Chemistry and Biochemistry, University of Colorado, Boulder, CO 80309.
* To whom correspondence should be addressed.
[⊗] Abstract published in *Advance ACS Abstracts,* January 1, 1997.

S1089-5639(96)02429-2 CCC: $14.00

in the stratosphere are large enough to make the IO self-reaction (4) important in ozone loss. Therefore, potential ozone loss must occur through the reactions of IO with ClO, BrO, and HO_2. However, the partitioning of reactive iodine between I and IO will be primarily determined by the rates of reactions 1 and 2, and thus, knowledge of the photolysis rate of IO is crucial to predict the effect of iodine compounds on stratospheric ozone.

The IO self-reaction has been studied previously.[8−13] In general, these studies have measured the decay rates of IO (produced in a number of different chemical systems) using visible absorption spectroscopy. While the reported values of k/σ (the ratio of the measured rate coefficient to measured IO cross section) for this reaction are in reasonable agreement (within a factor of 2), the use of different chemical systems and different values for the IO absorption cross section has complicated comparison of the previous results. The IO self-reaction could proceed via four different channels:

$$IO + IO \rightarrow I_2 + O_2 \quad (4a)$$

$$\rightarrow 2I + O_2 \quad (4b)$$

$$\rightarrow I + OIO \quad (4c)$$

$$IO + IO + M \rightarrow I_2O_2 + M \quad (4d)$$

In some earlier work,[9,10] IO was produced by reacting I atoms with excess ozone, and while complications due to aerosol formation arose, the results indicated that the rate coefficient for the IO self-reaction was pressure dependent. In this chemical system, channel 4b does not contribute to the loss of IO because it is regenerated via reaction 1. It was concluded that the disappearance of IO was through bimolecular (4a) and termolecular (4d) reactions. Subsequently, Sander[13] showed (by monitoring the production of I_2 following the photolysis of O_2/I_2 mixtures) that channel 4a constituted less than 5% of the total self-reaction and determined that the overall rate coefficient was pressure independent. However, he did identify a strong negative temperature dependence to the overall rate coefficient. His results also showed that the rate constant determined in the presence of ozone depended on pressure. A recent study of the IO self-reaction[11] confirmed that the decay of IO in the absence of ozone was pressure independent. Himmelmann et al.[14] have identified OIO in the photolysis of O_3/I_2 mixtures, suggesting that channel 4c may also be operating.

The current understanding of the kinetics of the IO self-reaction is that it proceeds via at least two bimolecular channels and one termolecular channel. The overall rate coefficient has a negative temperature dependence and, while the sum of channels 4a and 4d (and possibly 4c) is pressure dependent, the overall rate constant at room temperature is not, suggesting a compensating pressure dependence to the branching ratio. This type of complex reaction mechanism is seen in the self-reactions of ClO[15] and BrO.[16,17]

The UV−vis absorption spectrum of IO is continuous between 340 and 400 nm with vibrationally banded structure to longer wavelengths.[9,11,12,18] The absorption cross section at the peak of the (4,0) band has been determined at room temperature in a number of studies,[9−13] with reasonably good agreement. The temperature dependence of the IO cross section at this wavelength has been determined in only one previous study.[13]

This work describes a kinetic study of the self-reaction of IO and an investigation of the UV−vis absorption spectrum of IO with the aim of quantifying the role of iodine in the atmosphere.

2. Experimental Section

To determine the rate constant for the IO self-reaction, the absolute concentration of IO as a function of time must be measured. Laser flash photolysis with time-resolved visible absorption spectroscopy is the ideal technique for this study, allowing IO to be made rapidly and for its absolute concentration to be measured as it decays.

Apparatus. The flash photolysis apparatus used in this study has been fully described previously;[17] therefore, a brief description of the salient features (Figure 1) is given here. IO radicals were produced by laser photolysis and their concentrations measured using UV−vis spectroscopy. The apparatus consisted of a 91 cm long reaction cell with evacuated quartz windows. Flows of gases through the cell were controlled by stainless steel needle valves and measured by electronic mass-flow meters. The cell pressure was monitored using 10 and 1000 Torr calibrated capacitance manometers. The reaction cell was surrounded by a Pyrex jacket, through which a thermoregulation fluid was passed, enabling the cell temperature to be controlled to within 1 K in the range 200−400 K.

Photolysis light from an excimer laser was guided by dielectric mirrors through the cell collinearly with the spectroscopic analysis light. Analysis light was from a xenon arc lamp (75 W), a deuterium lamp (30 W), or a tunable diode laser operating at 427.2 nm. The analysis light sampled only the volume of the reaction cell through which the photolysis beam passed. The analysis light leaving the reaction cell was passed through suitable filters (ensuring that no photolysis laser light reached the detection optics) and directed onto the slits of either a 250 mm focal-length spectrometer coupled to a photomultiplier tube (PMT) or a 270 mm focal-length spectrograph coupled to a 1024-element diode array detector. The 427.2 nm laser beam was delivered to a photodiode detector.

The monochromator−PMT detection system was operated with entrance slits of 25 μm, giving a spectral resolution of 0.14 nm fwhm. The PMT signals were converted to absorptions using prephotolysis light intensities. The sensitivity of the PMT−monochromator system for a single integration was typically 0.001 absorption units for a signal-to-noise (S:N) ratio of unity.

The diode array−spectrograph system was operated with entrance slits of 10 μm, giving a spectral resolution of 0.44 nm fwhm. The total spectral coverage was approximately 120 nm. The wavelength scale of the diode array was calibrated with the emission from a mercury lamp. The diode array was electronically gated, enabling it to be switched on for short periods of time (e.g., 50 μs) following photolysis. Thus, "snapshots" of the transmitted spectral intensity could be recorded before and after the laser flash, allowing us to spectroscopically measure losses of reactants and the formation of products. The diode array detection system could typically measure absorbance changes of 0.01 for a single integration with a S:N ratio of unity.

The 427.2 nm light was produced by second harmonic generation (SHG) of a 854 nm extended cavity diode laser source, using temperature-tuned $KNbO_3$ for the doubling crystal. The laser line width was less than 100 kHz, verified by observations with an optical cavity. The laser wavelength was measured with a wavemeter to a precision of one part in a million. An optical ring cavity was used to enhance the fundamental IR in the 15 mm long $KNbO_3$ crystal. The blue SHG light was focused into a 20 meter optical fiber (single mode at 427 nm), which allowed for some flexibility in the position of the absorption cell relative to the diode laser setup.

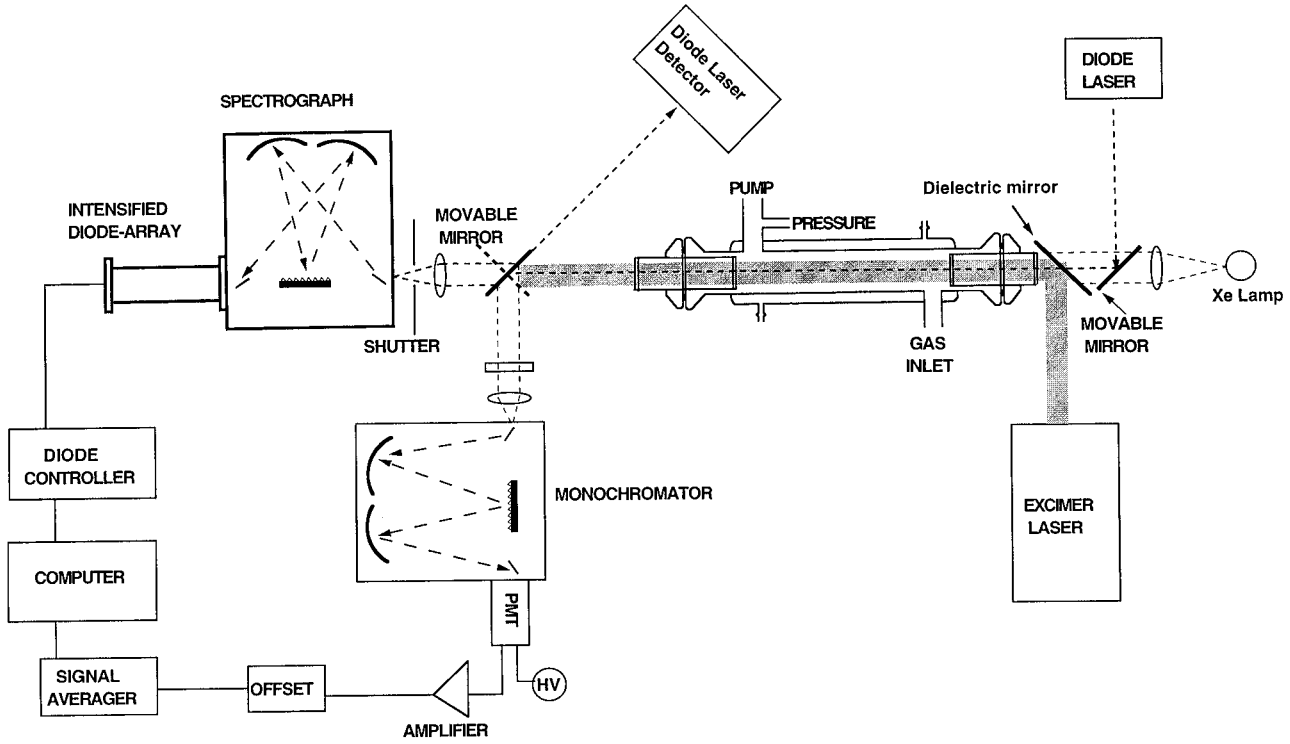

Figure 1. Schematic diagram of the pulsed photolysis apparatus

Although the intensity noise exhibited by diode lasers is often quite low relative to other types of light sources, the use of the optical buildup cavity and the optical fiber resulted in intensity noise on the 427 nm beam of a few percent. This noise was greatly reduced by using an electrooptical modulator for intensity stabilization. Approximately one-third of the power exiting the fiber was diverted by a beam splitter, detected, and used for a wide-band servo loop (1.5 MHz) to control the modulator. The remaining two-thirds of the power (about 0.5 mW), used to monitor the IO absorption, exhibited intensity fluctuations at or below the 10^{-6} level from dc out to 50 kHz. However, after the reaction cell, intensity fluctuations were an order of magnitude greater than this.

3. Method

Production of IO Radicals. IO radicals were produced in two ways. In the first method, N_2O was photolyzed at 193 nm in an excess of N_2, and the O atoms thus produced reacted with either I_2 or CF_3I to produce IO:

$$N_2O + h\nu(\lambda = 193\ \text{nm}) \rightarrow N_2 + O(^1D) \quad (7)$$

$$O(^1D) + N_2 \rightarrow N_2 + O(^3P) \quad (8)$$

$$O(^3P) + I_2 \rightarrow IO + I \quad (9)$$

$$O(^3P) + CF_3I \rightarrow IO + CF_3 \quad (10a)$$

$$\rightarrow \text{other products} \quad (10b)$$

In these experiments, the concentration of N_2 was high ($>1 \times 10^{19}$ molecules cm^{-3}), and the quenching of $O(^1D)$ to $O(^3P)$ was therefore complete (>99%) in 10 ns—essentially instantaneous on the time scale of the subsequent chemistry. In addition, the concentrations of I_2 and CF_3I were kept sufficiently high such that the formation of IO was fast ($<50\ \mu$s) relative to its subsequent reactions.

In the second system, mixtures of ozone and I_2 were photolyzed with the excimer laser operating at 308 or at 248 nm, and the IO was formed via the following processes:

$$O_3 + h\nu\ (\lambda = 308/248\ \text{nm}) \rightarrow O_2 + O(^1D) \quad (11a)$$

$$\rightarrow O_2 + O(^3P) \quad (11b)$$

$$O(^1D) + N_2 \rightarrow N_2 + O(^3P) \quad (8)$$

$$O(^3P) + I_2 \rightarrow IO + I \quad (9)$$

In both systems, the initial IO concentration was varied in the range $(1-30) \times 10^{12}$ molecules cm^{-3} by changing both the laser fluence and the concentration of the precursors (N_2O or O_3).

4. Results

To study the kinetics of the IO self-reaction by visible absorption spectroscopy, it was first necessary to determine the absorption cross sections of the IO radical in this region. The next section describes measurements of the absorption cross sections for IO and is followed by the results from the kinetic studies of the IO self-reaction.

(a) Spectroscopic Studies of IO. We first measured the absorption spectrum of IO between 340 and 480 nm using the diode array spectrometer. The absorption cross section at 427.2 nm was then measured, in separate experiments, to place the diode array spectrum on an absolute scale.

The IO Spectrum. IO was produced by the photolysis of N_2O in the presence of excess CF_3I. The diode array was gated to be "on" for 50 μs before and for 50 μs after the laser photolysis flash. The absorption due to IO was calculated from the relationship

$$A(\text{IO})\lambda = \ln[(I_0)\lambda/(I_t)\lambda] \quad (i)$$

where I_0 and I_t are the preflash and postflash intensities, respectively.

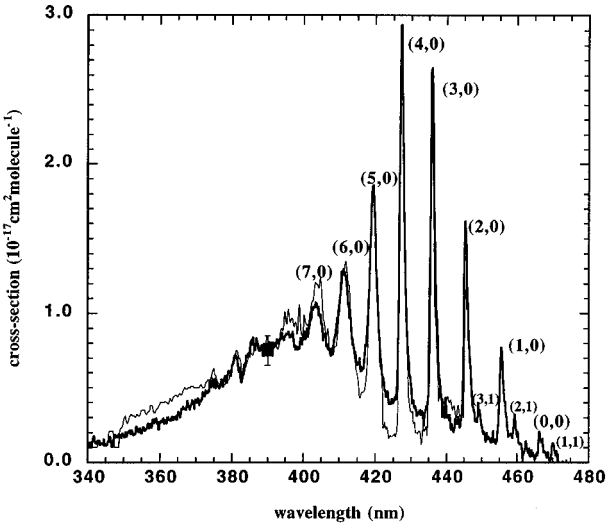

Figure 2. IO absorption spectrum: thick line, cross sections from this work; thin line, cross sections from Laszlo et al. The cross section from the PMT−monochromator measurement at 390 nm is given as a solid symbol (■).

The absorption spectrum for IO at 298 K (Figure 2) shows a smooth shoulder between 340 and 380 nm, beyond which some broad peaks are visible on top of the continuum. A progression of vibrational bands from the (7,0) band at 411 nm to the (0,0) band at 466 nm is also seen (see ref 19 for band assignments).

To ensure that the short-wavelength continuum in the spectrum was indeed due to IO, the temporal variation of the absorption at 427.2 nm was recorded using the monochromator−PMT system and compared to that measured at 390 nm under chemically identical conditions. The measured values of k_4/σ (the slopes of the second-order plots) were in the same ratio as the cross sections at the two wavelengths, suggesting that the absorption at 390 nm was indeed due to IO. It is unlikely that this absorption arises from any other species (e.g., I_2O_2) which would have a different temporal profile. In addition, if the absorption at 390 nm was due to I_2O_2, then its contribution should be expected to increase significantly at low temperatures. However the spectrum attributed to IO showed very little variation in shape with temperature. Our dual-wavelength study allowed the relative magnitude of the IO cross section at 427.7 and at 390 nm to be determined ($\sigma(\mathrm{IO})_{\lambda=427.2}/\sigma(\mathrm{IO})_{\lambda=390} = 4.7 \pm 0.2$). This is a useful check on the wavelength-dependent IO cross sections described below.

Kinetic studies, described later, were carried out by monitoring the absorption at the peak of the (4,0) band because the IO absorption cross section is largest here (ensuring maximum sensitivity to IO) and because the cross section of the other species (e.g., I_2) involved in the reactions are sufficiently small for them to have a negligible effect on the measured absorptions. The shape of this band was investigated at 298 K under high resolution using the tunable diode laser absorption system. IO was produced in the photolysis of I_2/N_2O mixtures, and the maximum absorption was measured at a range of wavelengths between 426.6 and 427.6 nm, under identical chemical conditions. With the assumption that the amount of IO produced was constant, the relative absorptions were plotted as a function of wavelength (Figure 3) to determine the shape of the (4,0) band. The (4,0) feature shows a very sharp edge on the short wavelength side and a broad "tail" on the long-wavelength side. It is clear from Figure 3 that no rotational fine structure exists in this absorption band.

Determination of the IO Absorption Cross Section at 427.2 nm. Various IO production schemes and quantification methods were employed during this study. IO production via the O + CF_3I reaction was the most precise and accurate and is presented first. The other two less precise methods provided supporting values and are described later.

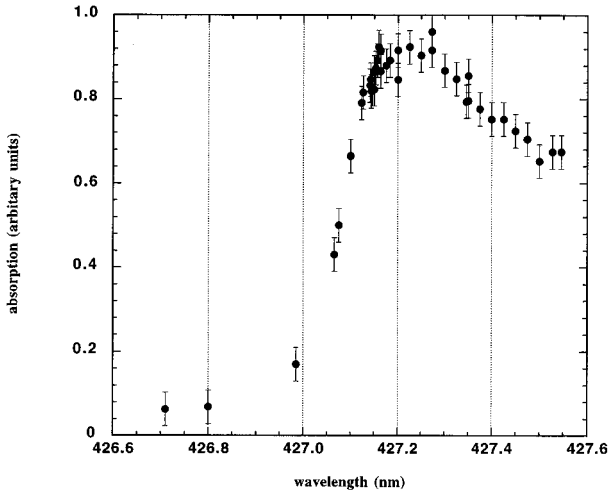

Figure 3. Shape of the (4,0) absorption band of IO under high resolution. The wavelengths are for vacuum.

Photolysis of N_2O/CF_3I. In these experiments, O atoms were produced by N_2O photolysis as described above. The concentration of O atoms was quantified by adding O_2 to the cell and monitoring the absorption due to the ozone formed via the reaction

$$O(^3P) + O_2 + M \rightarrow O_3 + M \qquad (12)$$

O_3 formation was monitored at 253.7 nm where the O_3 absorption cross section is well established and relatively temperature independent ($\sigma = 1.15 \times 10^{-17}$ cm^2 molecule^{-1} [20]). The O_2 was then replaced with CF_3I, and the absorption due to IO at the peak of the (4,0) band was monitored with the PMT−monochromator combination under conditions that were otherwise identical. An example of the absorption profiles at 427.2 nm (IO) and at 253.7 nm (O_3) obtained in these experiments is shown in Figure 4A.

Experiments performed by Gilles et al.[21] have shown that the yield (Φ) for IO in the reaction between O(^{3}P) and CF_3I is 0.86 ± 0.06 independent of temperature (between 370 and 254 K). To a first approximation, the IO cross sections can be determined using the following expression:

$$\sigma(\mathrm{IO}) = \frac{A(\mathrm{IO})\sigma(\mathrm{O_3})}{A(\mathrm{O_3})\Phi} \qquad \text{(ii)}$$

As seen in Figure 4A, the ozone absorption ($A(O_3)$) is constant and easily measured. In contrast, the absorption due to the IO initially produced is more difficult to quantify because, once formed, IO is consumed in self-reaction 4 and via reaction with O atoms:

$$O(^3P) + IO \rightarrow I + O_2 \qquad (13)$$

($k_{13} = (1.4 \pm 0.4) \times 10^{-10}$ cm^3 molecule^{-1} s^{-1} [11]). To account for this loss, the measured absorption profiles were analyzed using FACSIMILE[22] (a commercial numerical integration software package). In this approach, a chemical reaction scheme involving reactions 4, 10, and 13 was simulated, with the initial concentration of O atoms set equal to the measured $\Delta[O_3]$. The absorption cross section of IO and the rate coefficient of the IO self-reaction were then optimized to fit the observed decay

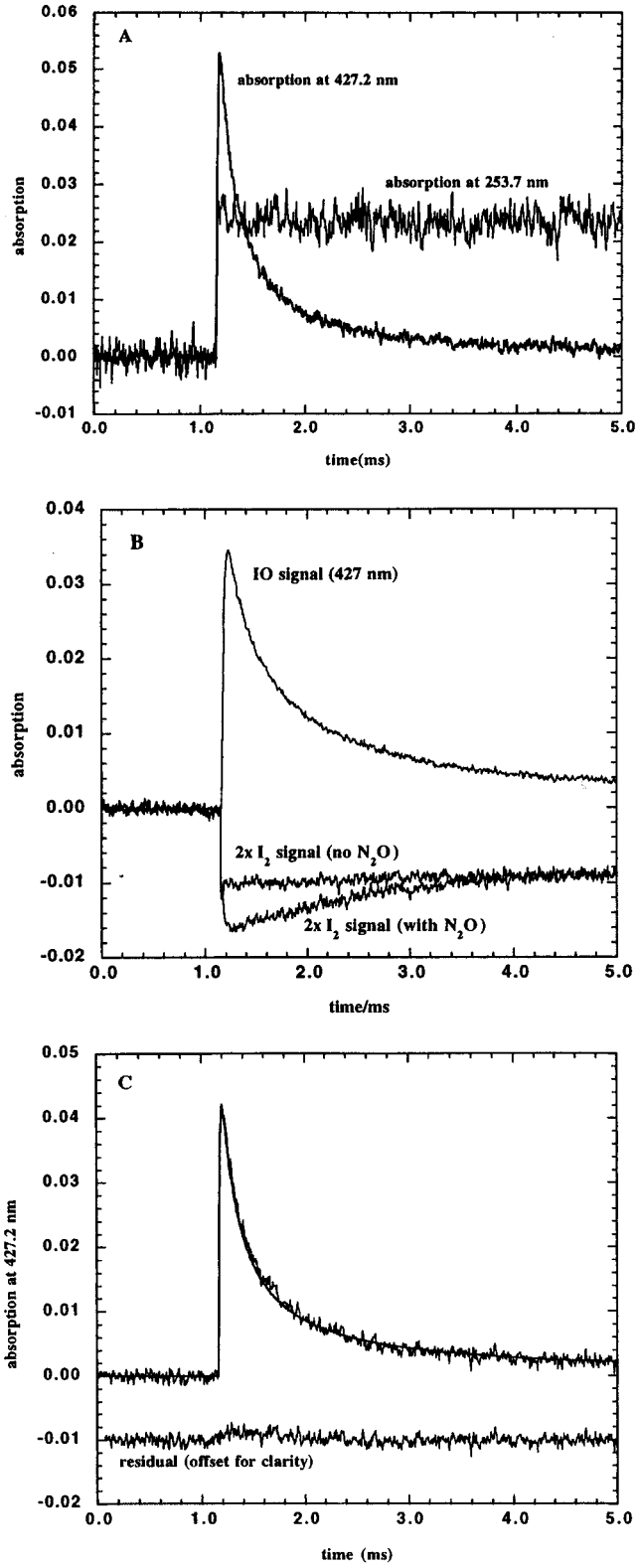

Figure 4. Determination of the IO cross section at 427.2 nm: (A) Absorption profiles of IO (427.2 nm) and ozone (253.7 nm); (B) profiles of IO (427.2 nm) and I_2 (500 nm), showing the I_2 photolysis component of the absorption signal. The I_2 absorption traces are multiplied by 2 for clarity. (C) Numerical fitting of the observed IO decays to a reaction scheme to determine the IO cross section. Residuals (data fit), offset for clarity, are also shown.

of IO. Figure 4C shows one such fit. For the conditions used in this study, the correction to the absorption cross section as calculated from expression ii was less than 10%. The IO absorption cross section was determined in this way at different temperatures, and the results are given in Table 1.

TABLE 1: IO Cross Sections at 427.2 nm from All Experiments[a]

system	temp/K	no. of runs	$[O]_0/10^{12}$ molecules cm^{-3}	IO cross section/ 10^{-17} cm^2 $molecule^{-1}$
N_2O/CF_3I	373	4	5−20	3.9 ± 0.1
	353	5		3.4 ± 0.1
	323	8		3.3 ± 0.1
	298	8		3.4 ± 0.1
	250	6		3.7 ± 0.2
	220	4		3.7 ± 0.1
	203	4		3.6 ± 0.2
O_3/I_2	298	16	0.5−5	3.5 ± 0.4
	275	4		3.7 ± 0.4
	253	4		3.1 ± 0.4
N_2O/I_2	298	13	5−15	3.3 ± 0.4

[a] Data from the N_2O/CF_3I system only was used in the recommendation. The given uncertainties are those due to random errors at the (1σ) level.

Weighted linear least-squares fitting to this data showed that the error in the temperature trend is much larger than the trend itself, and we therefore recommend an average temperature-independent value for the IO cross section at the peak of the (4,0) band head of $\sigma = (3.6 \pm 0.5) \times 10^{-17}$ cm^2 $molecule^{-1}$, where the error indicates the sum of both the estimated systematic errors (estimated as 10%) and the random errors (1σ).

Photolysis of N_2O/I_2. IO was produced in the N_2O/I_2 system as described above. The PMT−monochromator system was used to monitor absorptions at 427.2 nm (IO) and 500 nm (I_2) before and after the laser pulse. The change in the absorption at 500 nm was used to estimate the concentrations of I_2 removed via the $O + I_2$ reaction and, hence, the IO concentration. It was assumed that I_2 is the only absorber at 500 nm.

There are, however, a few problems associated with this method. I_2, which has a significant absorption cross section at 193 nm, was unavoidably photolyzed. To account for this, absorption profiles were recorded at 500 nm with only I_2 and N_2 in the cell; examples are shown in Figure 4B. It is clear from the figure that a large fraction of the I_2 is directly photolyzed. Further, N_2O can significantly attenuate the 193 nm laser fluence. Therefore, low N_2O concentrations had to be employed. Use of such low N_2O concentrations meant that the change in the I_2 absorption resulting from the $O + I_2$ reaction was only a fraction (10 −70%) of that due to the photolysis of I_2.

We noted some inconsistencies in the regeneration of I_2 in this reaction system. In the absence of N_2O, the I_2, once photolyzed, was regenerated presumably via the reaction

$$I + I + M \rightarrow I_2 + M \qquad (14)$$

The "return" of I_2 followed second-order kinetics yielding a bimolecular rate constant of 3×10^{-13} cm^3 $molecule^{-1}$ s^{-1} at a pressure of 520 Torr. On addition of N_2O, however, the rate of I_2 regeneration (via a bimolecular reaction) increased dramatically, giving a rate constant of 1.2×10^{-12} cm^3 $molecule^{-1}$ s^{-1} at 298 K and 520 Torr. Similar enhancement was also observed by Laszlo et al.[11] in the same chemical system. They attributed this enhancement to a reaction between I atoms and a product of the IO self-reaction. Numerical simulations showed that our observed enhancement in the I_2 regeneration rate cannot be due to the direct production of I_2 in the IO self-reaction because (a) the IO + IO reaction can only regenerate half the original I_2 lost (the other half having been I atoms) and (b) the temporal profiles of IO and I_2 do not match. Further, the I_2 signal was observed to return to prephotolysis values at long reaction times, indicating that in this reaction system there are no stable products other than I_2.

The above evidence points to some catalyzed regeneration of I_2 in this system. The most likely possibility is

$$IO + I + (M?) \rightarrow I_2O + (M?) \quad (15)$$

$$I + I_2O \rightarrow I_2 + IO \quad (16)$$

$$\text{net} \qquad 2I \rightarrow I_2$$

Indeed, the rate of the I_2 regeneration increased with the concentration of I atoms. If reaction 15 is termolecular, this mechanism would also explain the observation by Laszlo et al.[11] that the rate of regeneration of I_2 increased at higher pressures. Other species that could react with I atoms (OIO or I_2O_2) are not likely to cause *catalytic* regeneration of I_2.

Because of these complications, the IO cross section at 427.2 nm was determined by equating the difference in the initial amounts of I_2 lost in the I_2/N_2O and I_2-only photolysis (under optically thin conditions) to the amount of IO formed. The IO absorption signal was extrapolated to $t = 0$ and the cross section calculated from the following expression:

$$\sigma(IO)_{427\text{ nm}} = \left(\frac{A_{t=0}^{427\text{ nm}}(I_2, N_2O)}{A_{t=0}^{500\text{ nm}}(I_2, N_2O) - A_{t=0}^{500\text{ nm}}(I_2\text{ only})}\right)\sigma(I_2)_{500\text{ nm}} \quad \text{(iii)}$$

The room temperature cross section for I_2 at 500 nm[23] was taken to be 2.15×10^{-18} cm^2 molecule^{-1}.

The precision of the resulting IO cross section values was low, due to the difficulty in measuring the small signal due to the I_2 lost through the $O + I_2$ reaction. The room temperature value is $\sigma(IO, \lambda = 427.2\text{ nm}) = (3.3 \pm 0.7) \times 10^{-17}$ cm^2 molecule^{-1} where the error indicates the sum of both the estimated systematic errors (15% of the value) and the random errors (1σ). These measurements were restricted to 298 K and are in good agreement with our primary method.

Photolysis of O_3/I_2. In another set of experiments, IO was generated in the O_3/I_2 system where the decrease in the ozone absorption (at 253.7 nm) determines the concentration of O atoms (and therefore IO) produced. This system has also been used in previous studies.

We found that the mixture of I_2, O_3, and N_2 reacts "in the dark" to form a species that strongly attenuates the UV and visible light. This attenuation was significant at 308 and 253.7 nm and hence interfered with both photolysis and detection (253.7 nm was the wavelength used for ozone detection). Furthermore, as time progressed, a light brown film developed in the reaction cell and reduced the laser fluence, making experiments difficult.

To determine the source of the attenuation, the deuterium lamp/diode array system was used to measure the extinction in the range 230−370 nm. The extinction spectrum of the cell's contents was measured, first with O_3/N_2 only and then at increasing times after the addition of I_2. On adding I_2, the absorption due to O_3 dropped, and a new "absorption" appeared in the UV region. The ozone absorption continued to drop with time, and the new feature grew. Using the characteristic structure in the ozone absorption near 260 nm, the contribution of ozone to the observed spectrum was subtracted. The residual extinction (due to the reaction product) showed a very broad absorption, whose peak shifted to longer wavelengths with time (Figure 5). These results are consistent with the growth of an aerosol whose maximum Mie scattering cross section moves to longer wavelengths as the size of the aerosol particles increases. The unknown species showed a significant extinction

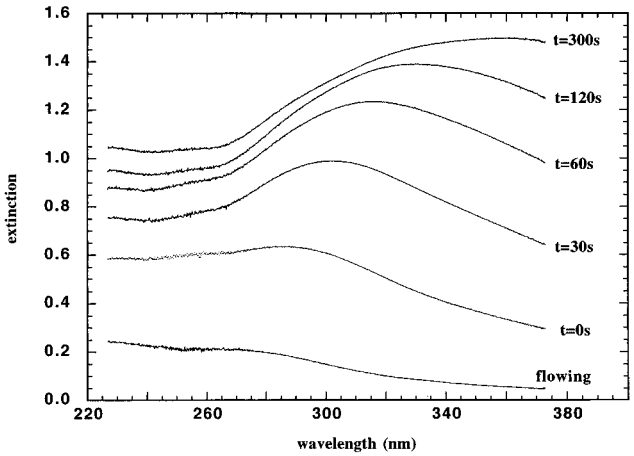

Figure 5. Extinction spectrum of the aerosol produced on mixing flows of I_2 and O_3. The spectrum marked "flowing" is that of the mixture flowing through the reaction cell. The other spectra were recorded at the indicated time intervals after stopping the flow of this mixture and demonstrate the growth of the aerosol.

to wavelengths as long as 500 nm. If we assume that the wavelength at the peak of the extinction spectrum is approximately equal to the radius of the particle, it appears that the particles grow from about 0.25 to about 0.4 μm in 5 min. The measured optical depth suggests a particle volume of 2×10^{-7} cm^3 per cm^3 of gas. This particle volume is consistent with the amount of ozone and I_2 lost from the gas phase.

Minimizing exposure to the deuterium lamp analysis light prior to the making each spectral measurement had a small effect on the growth of the absorber. However, reducing the temperature from 298 to 250 K dramatically reduced the extinction, suggesting that there is some thermal barrier to the formation of the aerosol. However, even at 250 K, the 'dark' reaction was sufficient to preclude meaningful measurements of the IO profiles.

Photolysis of ozone at 248 nm, where its cross section is significantly higher, allowed us to use very low ozone concentrations and thus minimize the problems due to aerosol formation. Further, use of a tunable diode laser at 427.2 nm allowed us to produce only small amounts of O and therefore to detect small amounts of IO. In these experiments, the laser fluence was calibrated using the photolysis of HNO_3:

$$HNO_3 + h\nu\ (\lambda = 248\text{ nm}) \rightarrow OH + NO_2 \quad (17)$$

and the NO_2 produced was monitored with the same diode laser ($\sigma_{427.2\text{ nm}}(NO_2) = 5.73 \times 10^{-19}$ cm^2 molecule^{-1}.[24] Small corrections to the measured value of $\Delta[NO_2]$ were made to account for the presence of a small amount of NO_3 which absorbs at 427.2 nm and is produced in the $OH + HNO_3$ reaction. The O atom concentration at a specific photolysis laser fluence was determined using the expression

$$[O]_0 = \frac{\sigma(O_3)\,\Phi(O_3)[O_3]\Delta[NO_2]}{\sigma(HNO_3)\,\Phi(HNO_3)[HNO_3]} \quad \text{(iv)}$$

where the quantum yields for O and NO_2 production from O_3 and HNO_3 photolysis at 248 nm, respectively, were assumed to be unity.[20] The O_3 and HNO_3 concentrations were determined via UV absorption measured using the diode array spectrometer. The O_3 and HNO_3 absorption cross sections at 248 nm were taken from ref 20. The IO cross sections were then determined from the measured IO absorption at 427.2 nm and the concentration of O atoms assuming quantitative conversion of O to IO (justified by the large excess of I_2). The IO

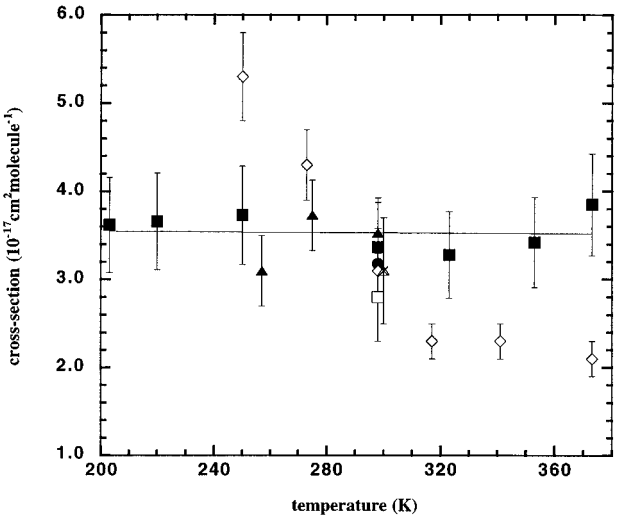

Figure 6. Cross sections for IO at the peak of the (4,0) absorption band as a function of temperature. Solid symbols indicate data from this study (■, N_2O/CF_3I system; ●, N_2O/I_2 system; ▲, the O_3/I_2 system). Open symbols are from previous work (□, Laszlo et al.; ◇, Sander; ×, Cox et al.; △, Stickel et al.). The line shows the weighted linear least-squares fit to the N_2O/CF_3I system.

cross sections were measured at 298, 275, and 257 K, and the results are given in Table 1.

The IO Absorption Spectrum. The absorption cross sections of IO at 427.2 nm, the (4,0) band head, determined by the three methods at room temperature are shown in Figure 6. Also shown are the cross sections measured between 373 and 203 K. As noted earlier, it is clear that the cross sections are essentially independent of temperature. To determine the cross sections at other wavelengths, the IO spectrum, measured with the diode array, was placed on an absolute scale using the value at 427.2 nm. To account for the difference in the wavelength resolution of the PMT and diode array spectrometer detection systems, the high-resolution IO spectrum measured with the tunable diode laser (shown in Figure 3) was degraded by convolving it with the instrument function of the diode array (approximated by a Gaussian function with a fwhm = 0.44 nm). This approach showed that the cross section at the peak of the (4,0) band in the diode array spectrum should be 0.83 of the value determined with the PMT detection. The diode array spectrum was then scaled to this value to give the IO cross sections as a function of wavelength (Figure 2). The value of the IO cross section determined at 390 nm by monitoring the decay of IO at 427.2 and 390 nm under identical conditions (as described above) is also shown in Figure 2 and is in excellent agreement with the diode array data.

Using a temperature-independent cross section at the peak of the (4,0) band, the diode array spectra of IO recorded at a variety of temperatures (298, 273, 253, 233, 213, and 203 K) were normalized at 427.2 nm. The temperature dependence of the rest of the spectrum was then determined. This approach showed that in the range 340 and 440 nm the cross sections changed by less than 10% between 298 and 203 K.

(b) Kinetics of the Self-Reaction of IO Radicals. In most of the kinetic studies described here, the IO concentration was monitored using the (4,0) absorption band. However, as a check, in one series of experiments, we monitored IO via two different methods: diode array absorption and single-wavelength monitoring under otherwise identical conditions. The PMT was used to monitor the absorption at the peak of the (4,0) band, and the gated diode array was used to measure the absorption spectrum in the range 340−480 nm at fixed time intervals before and after the photochemical production of IO. The measured

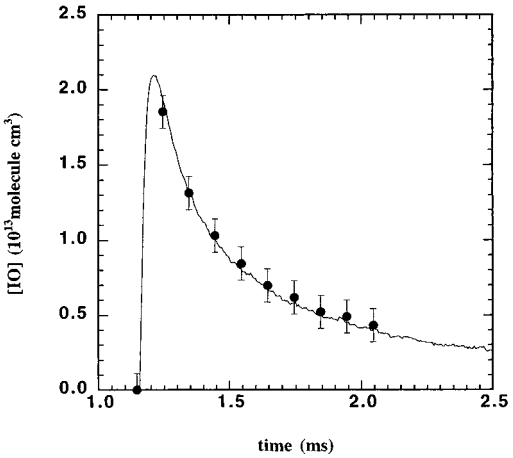

Figure 7. Comparison of the IO decay obtained using the PMT−monochromator at 427.2 nm (line) compared with that from the gated diode array (●), where the entire spectrum was monitored as a function of time.

spectral changes were converted into IO concentrations by fitting a reference IO spectrum to the measured IO spectrum (using a linear least-squares technique). The temporal profiles of IO obtained from the absorption at 427.2 nm are identical, within the error bars, to those obtained from the gated diode array (Figure 7). Because the diode array measurement discriminates against any absorption not due to IO, the agreement clearly shows that the absorption at 427.2 nm is solely due to IO.

Photolysis of N_2O in the Presence of I_2. The decay of IO formed in the N_2O/I_2 system was monitored at 427 nm using the monochromator−PMT detection system, and the cross section recommended above was used to convert the measured IO absorption into a concentration as a function of time. The loss of IO through its self-reaction is given by the rate equation:

$$-\mathrm{d[IO]d}t = 2k_4[\mathrm{IO}]^2 \qquad \text{(v)}$$

whose integrated form is

$$\frac{1}{[\mathrm{IO}]_{t=t}} = \frac{1}{[\mathrm{IO}]_{t=0}} + 2k_4t \qquad \text{(vi)}$$

At and above room temperature, the IO decays were observed to be strictly second-order (i.e., plots of 1/[IO] versus time were linear). The rate constants were obtained from the slopes of the second-order plots (such as those shown in Figure 8, lines a and b) using a weighted linear least-squares analysis. The second-order rate coefficient did not change with the initial concentration of IO (over the range (5−20) × 10^{12} molecules cm^{-3}).

At low temperatures, some deviation from second-order kinetic behavior was observed; the second-order plots had an upward turning tail (e.g., Figure 8, line c). As the IO concentrations were increased, this deviation became more pronounced. Here the loss of IO obeyed a mixture of first- and second-order kinetics. The observations are consistent with the reaction of IO with a product of the self-reaction

$$\mathrm{IO} + \mathrm{IO} \rightarrow \text{product 1} \qquad (4)$$

$$\mathrm{IO} + \text{product 1} \rightarrow \text{product 2} \qquad (18)$$

The hypothetical reaction 18 would explain the first-order loss component of IO. This first-order loss would be largest at long reaction times where the [product 1]/[IO] ratio is greatest. Numerical integration of reactions 4 and 18 was used to simulate

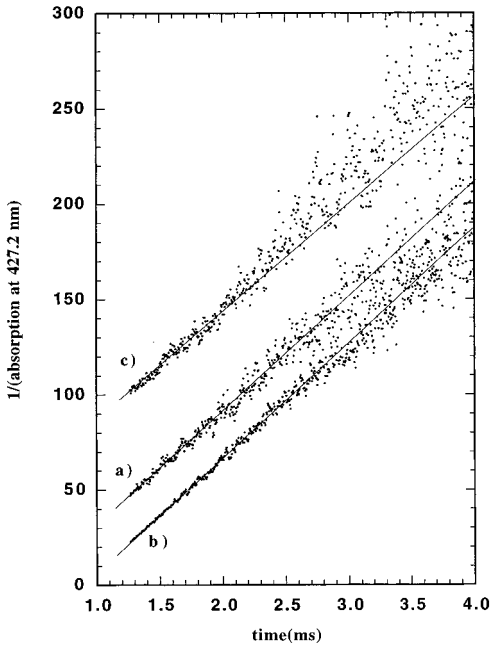

Figure 8. Second-order plots for the decay of IO. Lines a and b display data from two different initial IO concentrations; line c shows the non-second-order kinetic behavior observed at low temperatures.

TABLE 2: Rate Constants for the IO Self-Reaction as a Function of Temperature[a]

system	temp/K	no. of runs	conditions/ molecules cm^{-3}	k(IO+IO)/ 10^{-11} cm^3 $molecule^{-1}$ s^{-1}
N_2O/I_2	373	8		9.5 ± 0.3
	353	12		9.9 ± 0.4
	323	12	$[O]_0 = (5-30) \times 10^{12}$	11.1 ± 0.5
	298	15	$[I_2] = (1-5) \times 10^{14}$	10.1 ± 0.4
	273	17		9.8 ± 0.4
	261	7		9.4 ± 0.4
	250	12		9.4 ± 0.6
O_3/I_2	298	16	$[O]_0 = (2-15) \times 10^{12}$	7.0 ± 1.0
	275	4	$[I_2] = (1-7) \times 10^{14}$	7.2 ± 1.0
	257	4		7.7 ± 1.0

[a] The given uncertainties are those due to random errors at the (1σ) level.

IO decays resulting from such a mixed first- and second-order kinetic scheme and the fits to the observed IO profiles were improved significantly over the second-order-only mechanism. In order to determine the rate constant for the IO self-reaction at all temperatures below ambient, FACSIMILE was used to optimize the rate constants for reactions 4 and 18 to best fit the observed decays. Careful checks were performed to ensure that the returned values were unique. In these tests, the optimized value for k_4 was reduced or increased by 10% and then FACSIMILE used to resimulate the decay profile with this new value. The fit to the IO decay was measurably worse. In addition, rate constants for reactions 4 and 21 were varied to fit up to eight IO decays simultaneously, and the optimized values for k_4 and k_{18} were found to agree with the values returned from fitting the decays individually.

The rate coefficients for the IO self-reaction measured in the N_2O/I_2 system using both the graphical approach ($T \geq 298$ K) and the FACSIMILE analysis ($T < 298$ K) are given in Table 2 and are displayed in Figure 9.

Photolysis of Ozone at 248 nm in the Presence of I_2. A series of experiments were performed with ozone and iodine concentrations sufficiently low ($[O_3] = (1-5) \times 10^{13}$ molecules cm^{-3}, $[I_2] = (1-7) \times 10^{14}$ molecules cm^{-3}) that the aerosol production was significantly reduced. The decay of IO produced by the reaction of O atoms with I_2 was monitored at 427.2 nm with the tunable diode laser absorption system at three temperatures (298, 275, and 257 K). The second-order plots from these experiments displayed significant curvature over a time scale of about 8 ms, resulting from the regeneration of IO (via reaction 1 at low IO:O_3 ratios). However, reasonable linearity was observed over the first 2 ms of the decay, and the slope in this region was used to determine the rate coefficient. This slope showed some dependence on the laser fluence used in the experiments (approximately a 10% increase in the measured rate coefficient for a doubling of the laser fluence). This effect was not fully understood and not pursued further. The average values of the measured rate coefficients from this system are also given in Table 2.

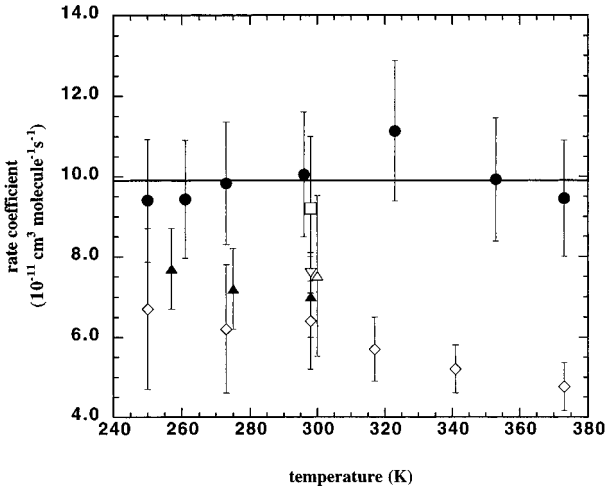

Figure 9. Rate coefficients for the IO self-reaction as a function of temperature. Solid symbols indicate measurements made in this work (●, the N_2O/I_2 system; ▲, the O_3/I_2 system). Open symbols indicate rate coefficients from other work (note that these rate coefficients have been normalized to our cross section values): (□, Laszlo et al. (N_2O/I_2); ▽, Laszlo et al. (O_3/I_2); ◇, Sander (O_2/I_2); △, Stickel et al. (O_3/I_2)). The bold line shows the rate coefficient recommendation from this work.

Even though production of IO via the O + CF_3I reaction was the best method for measuring the IO cross sections, we did not employ this source for studying the IO kinetics. The secondary reactions of the CF_3 radical produced led to faster depletion of IO. However, the enhanced IO removal in this system does not affect the accuracy of the measured IO absorption cross sections.

Reaction Products. The gated diode array spectrometer was used to ascertain whether any products of the IO self reaction (in the I_2/N_2O system) could be observed spectroscopically between 340 and 900 nm and at temperatures between 250 and 373 K. No absorptions were detected ($[X]\sigma_X < 5 \times 10^{-5}$) other than those arising from the production of IO and the loss of I_2. This is in agreement with the measurements of the I_2 absorption at 500 nm in this system described above. At long reaction times, all the I_2 that had been removed in the laser photolysis returned. The PMT detection system was also used to follow the generation of I_2 in the CF_3I/N_2O reaction system in an attempt to determine the fraction of the IO self-reaction that yields I_2. The low absorption cross sections for I_2 made the sensitivity to I_2 formation low, but the measurements suggest an upper limit of 30% to the reaction channel 2a giving I_2.

5. Discussion

IO Spectrum. The cross section for IO at the peak of the (4,0) band in its visible absorption spectrum has been determined

as a function of temperature. The cross sections are independent of temperature between 373 and 203 K, and we recommend the value $\sigma(427.2\text{ nm}) = (3.6 \pm 0.5) \times 10^{-17}$ cm^2 molecule^{-1} where the error indicates the sum of random (1σ) and systematic errors. The shape of this absorption band was also investigated under high resolution (100 kHz) and shows no discernible rotational fine structure. The IO spectrum between 340 and 480 nm was recorded, and the cross section measured at 427.2 nm was used to place this spectrum on an absolute scale.

The room temperature IO cross section at the peak of the (4,0) band measured here lies within the error bars of previous measurements (Figure 6). However, the cross section measured here is 5−20% higher than the other values. Cox and Coker[9] and Jenkin and Cox[10] measured the cross sections at 426.9 nm, close to the steep shoulder of the (4,0) band (Figure 3), and thus it is possible that their lower values result from contributions from the valley to shorter wavelengths. The discrepancy between the other studies and ours could arise from the consumption of O atoms in the interfering (O + IO) and (O + O_2) reactions. In previous studies it was assumed that O atoms were quantitatively converted to IO. Sander,[13] Laszlo et al.,[11] and Stickel et al.,[12] did not take into account the O + IO reaction in the determination of the IO cross sections. In the work of Sander and of Stickel et al., the reaction between O and O_2 may have depleted O atoms. Both reactions would make $[IO]_0 < [O]_0$ and would lead to an overestimate of the nascent IO concentration and therefore an underestimate of the IO cross section. In the present study, the effect of the O + IO reaction was taken into account, and no O_2 was present. Another difference between this work and that of Laszlo et al.[11] is the spectral resolution. Laszlo et al. used 0.3 nm fwhm compared to our resolution of 0.14 nm. Therefore, their measured cross section at the (4,0) band head should be about 10% lower than ours.

Sander[13] published the only previous measurement of the IO cross sections as a function of temperature, and there is a significant difference between his data and ours. Sander reported that the IO cross section increased dramatically as the temperature decreased: $\sigma = 2.1 \times 10^{-17}$ cm^2 molecule^{-1} at 373 K, increasing to 5.3×10^{-17} cm^2 molecule^{-1} at 250 K. No statistically significant temperature dependence was measured here in either the (N_2O/CF_3I) or (I_2/O_3) IO production systems. While no obvious explanation for this discrepancy presents itself, the large increase in σ reported by Sander is not consistent with the measurements of the IO produced from the O + CF_3I reaction combined with the quantum yields for this reaction measured by Gilles et al.[21] If the cross section measured by Sander at 250 K were correct, the measured quantum yield for this reaction would have been approximately 0.35, significantly below the lower error limit of ($\Phi = 0.86 \pm 0.06$) quoted by Gilles et al. In addition, we do not see a significant temperature dependence to the cross section using a completely different IO source (the I_2/O_3 system). An increase in the absorption cross section at the peak of the (4,0) band might be expected with decreasing temperature, due to the changing populations of both the vibrational and rotational states. The change in the vibrational populations alone would be expected to make only a small contribution over this temperature range (<7%), and while the contributions from rotation could be larger, their magnitude is uncertain due to the predissociative nature of the (4,0) band.

The overall shape of the IO absorption spectrum (Figure 2) has been recorded with the diode array spectrometer as a function of temperature. The spectrum is smooth between about 340 and 370 nm, beyond which some structure is visible in the spectrum. The (0,0) to (7,0) vibrational bands can be observed in the spectrum, and the (1,1) (2,1), and (3,1) hot bands can also be seen. The room temperature IO spectrum measured here is in reasonable agreement with the most recent study of Laszlo et al.[11] though some subtle differences do present themselves. The larger peak-to-trough cross section differences in the Laszlo et al. spectrum probably result from the higher spectral resolution used in their study over that of our diode array system. In addition, while the broad spectral features between 380 and 410 nm show qualitative similarity, there are discrepancies in the cross section values of up to 30% in this region. Laszlo et al. had to measure the IO absorption at each wavelength in separate experiments to " build up" their spectrum. This approach would be sensitive to small changes in experimental conditions with time and could explain some of the discrepancies.

Our measurements of the IO spectrum as a function of temperature, coupled with a knowledge of the temperature dependence of the cross section at the peak of the (4,0) band, show that the IO spectrum is relatively insensitive to temperature. Absorption cross sections between 340 and 440 nm, averaged over 5 nm intervals, change by less than 10% between 298 and 203 K.

Reaction Kinetics and Mechanism. Rate coefficients for the self-reaction of IO radicals were measured here in two distinct chemical systems. These coefficients are compared with the values from previous studies in Figure 9. In the figure, previous determinations of the rate constants have all been normalized to the IO cross sections measured here (using the k/σ values) to ensure that the comparison between the various measurements is not biased by the difference in the cross sections used. In normalizing the data from Sander and Stickel et al., our cross section was not corrected for the differences in instrument resolution, because their resolutions were very similar to or better than ours. To normalize the Laszlo et al. data, our cross section was degraded to match their lower spectral resolution.

The rate coefficient for the sum of all channels of the IO self-reaction (potentially 4a−4d) is obtained in the experiments where the decay of IO produced in the I_2/N_2O system was monitored. The conclusion of the present work is that this rate coefficient shows no statistically significant temperature dependence ($250 > T > 320$ K), and we quote an average value of $k_4 = (9.9 \pm 1.5) \times 10^{-11}$ cm^3 molecule^{-1} s^{-1} (where the error incorporates the random errors in the slopes of the second-order plots (1σ) and the error in the absorption cross section). Our room temperature rate constant is in excellent agreement with that determined by Laszlo et al.[11] when their value is normalized to the IO cross section measured here. However, our kinetic data significantly differs from that of Sander.[13] In Sander's work, IO was produced via the photolysis of O_2 in the presence of I_2. It seems likely that the rate coefficients measured in his system would also represent the sum of all the self-reaction channels. However, Sander's rate coefficient at room temperature is much lower than ours (by almost a factor of 2), and its temperature dependence is large and negative. This apparent difference arises mainly from the highly temperature-dependent IO cross sections measured and used by Sander. If Sander's values are normalized to our cross section (as in Figure 9), his room temperature rate coefficient is only 30% lower than that determined here; however, a slight negative temperature dependence would still persist.

The rate coefficients determined in the I_2/O_3 system are smaller than those in the I_2/N_2O system. For example, the rate coefficient at room temperature is approximately 30% lower when ozone is present. Previous studies of the IO self-reaction

in ozone have shown that the measured rate coefficient is reduced because of the regeneration of IO in reaction 1. However, under the conditions employed here, the ozone concentrations were too low to allow such IO recycling. Thus, while these results are 25−30% lower than those obtained in the N_2O/I_2 system, due to the fluence dependence of the measured rate coefficients and a less extensive data set, we do not use these values in our recommendation.

In agreement with the results of Sander and of Laszlo et al., the overall IO self-reaction rate coefficient (k_4) was observed to be pressure independent. However, previous measurements of the decay of IO (Sander and Jenkin et al.) in excess ozone have shown a significant pressure dependence, and this is the basis for the proposed termolecular channel (4d). Sander also observed an absorber in his work which was tentatively identified as the IO dimer, I_2O_2. No spectroscopic evidence for I_2O_2 was obtained in our experiments, but it is possible that it was removed in our N_2O/I_2 experiments by a reaction with iodine atoms.

By monitoring I_2 production in the CF_3I/N_2O system, we place an upper limit of 30% upon channel 4a (giving I_2 and O_2). Both Sander and Laszlo et al. report that this channel constitutes less than 5% of the total reaction. Therefore, we adopt their value of 5% for the yield of channel 4a. Recent work by Himmelmann et al.[14] has provided spectroscopic evidence for OIO following the photolysis of molecular iodine in the presence of ozone. Although the exact source of the OIO is not known, it is possible that OIO is a product of the IO self-reaction. However, it was not observed in this study, possibly because the high I atom concentrations destroyed OIO. If OIO is indeed formed and the reaction ($I + OIO \rightarrow 2IO$) removes it, then our overall self-reaction rate coefficient would be a lower limit, as channel 4c would not contribute to the loss of IO.

The overall mechanism of the IO self-reaction is still somewhat uncertain due to the paucity of kinetic data on the individual reaction channels. The overall rate coefficient for the self-reaction (k_4) is temperature independent in the range 373−250 with a value of $k_4 = (9.9 \pm 1.5) \times 10^{-11}$ cm^3 molecule^{-1} s^{-1}. The channel giving I_2 and O_2 constitutes less than 5% of the total reaction[13,11] ($k_{4a} \leq 5 \times 10^{-12}$ cm^3 molecule^{-1} s^{-1}). Rate coefficients measured in excess ozone are for the channels of the IO self-reaction that do not give I atoms. Thus, k_{obs}(excess ozone)/k_{obs}(no ozone) can be equated to $(k_{4a} + 0.5k_{4c} + k_{4d})/k_4$. This ratio was determined to be approximately 0.83 by Laszlo et al. and 0.56−0.83 (depending on the pressure) by Sander. Thus, $(k_{4b} + 0.5k_{4c}) = (1.7-4.4 \pm 1.0) \times 10^{-11}$ cm^3 molecule^{-1} s^{-1}. Assuming that no other reaction channels are operating, we can derive that $(k_{4d} + 0.5k_{4c}) = (5.0 \text{ to } 7.7 \pm 1.0) \times 10^{-11}$ cm^3 molecule^{-1} s^{-1}. These values imply that the formation of the IO dimer (I_2O_2) is the dominant channel in the IO self-reaction. Thus, I_2O_2 may well have a significant atmospheric role, particularly in the troposphere.

We have also seen some evidence for catalytic regeneration of I_2 from I atoms in the N_2O/I_2 system, possibly through the formation of I_2O. In addition, our data suggest that IO reacts with a product of the IO self-reaction at low temperature. If OIO is indeed formed in channel 4c, it is possible that such a reaction is between IO and OIO and gives I_2O_3.

Atmospheric Implications. The kinetic parameters measured here show that the self-reaction of IO radicals is fast and that the major products are likely to be the IO dimer and iodine atoms. The overall rate constant of the IO self-reaction is significantly higher (approaching a factor of 2) than the value recommended by DeMore et al.[20] and used in the most recent modeling study.[4] If the UV−vis absorption spectrum of the IO dimer (in terms of cross section and wavelength range) follows the trend set by Cl_2O_2 and Br_2O_2, then it is likely that the IO dimer will be rapidly photolyzed everywhere in the sunlit atmosphere. If we assume the photolysis products lead to 2I and O_2 (by analogy with Cl_2O_2), then three channels of the IO self-reaction (4a, 4b, and 4d) will lead to catalytic destruction of ozone in the atmosphere. The rate constants published here for the self-reaction of IO radicals will therefore increase the predicted iodine-catalyzed ozone depletion in the troposphere, especially in areas of the atmosphere where the mixing ratio of CH_3I is elevated. In addition, these results heighten the importance of the IO self-reaction relative to the $IO + HO_2$ reaction within the IO_x cycle.

TABLE 3: Atmospheric Photolysis Rates for IO as a Function of Altitude and Solar Zenith Angle (SZA)

SZA (deg)	photolysis rate (s^{-1})			
	0 km	10 km	20 km	30 km
16	0.24	0.30	0.29	0.29
45	0.21	0.29	0.29	0.29
60	0.18	0.27	0.28	0.28
90	0.003	0.01	0.08	0.17

Atmospheric Photolysis Rates. The absorption cross sections measured here and a solar spectrum from Minschwaner et al.[25] (for a latitude of 40° at the summer solstice and with a total ozone column of 330 DU) were used to calculate the photolysis rates for IO for a variety of altitudes and solar zenith angles. In these calculations, the quantum yield for IO photodissociation was assumed to be unity throughout the absorption spectrum. The smooth nature of the IO spectrum below 400 nm suggests that the electronic transition leads to dissociation. Further, LIF studies of the (4,0), (3,0), (2,0), (0,0), and (2,1) bands (see for example ref 26) suggest that dissociation from the states accessed at these wavelengths is very rapid. Thus, use of unit photodissociation quantum yield for IO is justified. The calculated atmospheric photolysis rates (using 10 nm wide integration bins between 340 and 480 nm) are given in Table 3.

The values in the table are in excellent agreement with that reported by Laszlo et al., who gave a value of 0.28 s^{-1} for the IO photolysis rate at a SZA of 40°. The calculated *J*-values show that, as long as there is sunlight, IO is rapidly photodissociated. Photolysis is the most rapid process converting IO to I, being faster than reaction of IO with NO for typical NO concentrations. Further, the rapid photodissociation of IO coupled with the relatively slow reaction of I with O_3 means that I atoms form a significant proportion (about 30%) of total atmospheric iodine. Thus, I atoms may also be important initiators in the oxidation of certain atmospheric species.

Acknowledgment. The authors thank Edward Lovejoy for helpful discussions. M. Harwood thanks CIRES, University of Colorado, for the award of a Visiting Fellowship. This work was funded in part by the National Aeronautics and Space Administration's Mission to Planet Earth program from the Upper Atmosphere Research Program.

References and Notes

(1) Moyers, J. L.; Duce, R. A. *J. Geophys. Res.* **1972**, *79*, 5229.
(2) Zafiriou, O. C. *J. Geophys. Res.* **1980**, *79*, 2730.
(3) Chameides, W. L.; Davis, D. D. *J. Geophys. Res.* **1980**, *85*, 7383.
(4) Davis, D.; Crawford, J.; Liu, S.; McKeen, S.; Bandy, A.; Thornton, D.; Rowland, F.; Blake, D. *J. Geophys. Res.* **1996**, *101*, 2135.
(5) Solomon, S.; Garcia, R. R.; Ravishankara, A. R. *J. Geophys. Res.* **1994**, *99*, 20491.

(6) Barrie, L. A.; Bottenheim, J. W.; Hart, W. R. *J. Geophys. Res.* **1994**, *99*, 25.

(7) Stolarski, R. S.; Bloomfield, P.; MacPeters, R. D.; Herman, J. R. *Geophys. Res. Lett.* **1991**, *18*, 1015.

(8) Clyne, M. A. A.; Cruse, H. W. *Trans. Faraday Soc.* **1970**, *66*, 2227.

(9) Cox, R. A.; Coker, G. B. *J. Phys. Chem.* **1983**, *87*, 4478.

(10) Jenkin, M. E.; Cox, R. A. *J. Phys. Chem.* **1985**, *89*, 192.

(11) Laszlo, B.; Kurylo, M. J.; Huie, R. E. *J. Phys. Chem.* **1995**, *99*, 11701.

(12) Stickel, R. E.; Hynes, A. J.; Bradshaw, J. D.; Chameides, W. L.; Davis, D. D. *J. Phys. Chem.* **1988**, *92*, 1862.

(13) Sander, S. P. *J. Phys. Chem.* **1986**, *90*, 2194.

(14) Himmelmann, S.; Orphal, J.; Bovensmann, H.; Richter, A.; Ladstatter-Weissenmayer, A.; Burrows, J. P. *Chem. Phys. Lett.* **1996**, *251*, 330.

(15) Nickolaisen, S. L.; Friedl, R. R.; Sander, S. P. *J. Phys. Chem.* **1994**, *98*, 155.

(16) Harwood, M. H.; Rowley, D. M.; Freshwater, R. A.; Jones, R. L. *J. Phys. Chem.*, in press.

(17) Mauldin, R. L. I.; Wahner, A.; Ravishankara, A. R. *J. Phys. Chem.* **1993**, *97*, 7585.

(18) Durie, R. A.; Ramsay, D. A. *Can. J. Phys.* **1958**, *36*, 35.

(19) Coleman, E. H.; Gaydon, A. G.; Vaidya, W. M. *Nature* **1948**, *162*.

(20) DeMore, W. B.; Sander, S. P.; Goldan, D. M.; Hampson, R. F.; Kurylo, M. J.; Howard, C. J.; Ravishankara, A. R.; Kolb, C. E.; Molina, M. J. Chemical Kinetics and Photochemical Data for use in Stratospheric Modeling, Jet Propulsion Laboratory, 1994.

(21) Gilles, M. K.; Turnipseed, A. A.; Talukdar, R. K.; Rudich, Y.; Villalta, P. W.; Huey, L. G.; Burkholder, J. B.; Ravishankara, A. R. *J. Phys. Chem.* **1996**, *100*, 14005.

(22) *FACSIMILE*; Malleson, A. M.; Kellet, H. M.; Myhill, R. G., Sweetenham, W. P., Eds.; AERE Harwell Publications: Oxfordshire, 1990.

(23) Calvert, J. G.; Pitts, J. N. *Photochemistry*; John Wiley & Son: New York, 1966.

(24) Harder, J. W.; Brault, J. W.; Johnston, P. V.; Mount, G. H. *Submitted to J. Geophys. Res.*, in press.

(25) Minschwaner, K., private communication.

(26) Turnipseed, A. A.; Gilles, M. K.; Burkholder, J. B.; Ravishankara, A. R. *Chem. Phys. Lett.* **1995**, *242*, 427.